Monofluoro-ether electrolyte design with reduced Li⁺-anion coordination enables fast-charging ultrahigh-voltage lithium metal batteries

Digen Ruan[1,#], Lijiang Tan[1,#], Shunqiang Chen[1], Jiajia Fan[1], Qingshun Nian[1], Li Chen[1,2], Zihong Wang[1], Xiaodi Ren[1,*]

[1]School of Chemistry and Materials Science, University of Science and Technology of China, Hefei 230026, China

[2]Key Laboratory of Structure and Functional Regulation of Hybrid Materials, Anhui University, Hefei, 230601, China

Corresponding author email: xdren@ustc.edu.cn

[#]These authors contributed equally: Digen Ruan, Lijiang Tan

Abstract

Ether-based electrolytes are particularly useful for lithium metal batteries (LMBs) and have shown improved anodic stability with the high concentration design. Nevertheless, the vaunted anion-reinforced solvation in concentrated electrolytes has non-negligible adverse effect on ion conduction and battery rate performance. Here, we propose a new solvent design strategy of ether monofluorination to tune the Li⁺-anion interaction for fast-charging LMBs. With the highly polar monofluoro functional groups, the ether-based electrolyte not only exhibits excellent high oxidation stability due to the strong electron-withdrawing effect of F, but also has a greatly increased ionic conductivity because of reduced anion coordination. The unique solvation structure also enables the formation of robust and highly conductive interphases at both the Li anode and NMC811 surfaces. High Li CEs (~99.4%) and stable long-term cycling with low overpotential under ultrahigh current densities (10 mA cm⁻²) could be achieved for Li anode. Li‖NMC811 cells exhibit outstanding cycling performance under ultrahigh cut-off voltages of 4.6 V and 4.7 V, or at high current densities (5.1 mA cm⁻²). This work provides critical insights into the ion-solvent interactions in the solvation complex and their profound influence on the battery electrochemical performances.

Introduction

High-voltage Li metal batteries (LMBs) are regarded as one of the most promising next-generation energy storage systems because of their high energy densities.[1] Nevertheless, the highly active Li metal anode is notorious for its low Coulombic efficiency (CE), poor cycling performance and dendritic growth, especially under fast-charging conditions.[2, 3] At the same time, with the increase of Ni content and cut-off charging voltage for lithium nickel manganese cobalt oxide (NMC) cathodes, severe side reactions with the electrolyte would induce faster capacity decay. [4-6] Therefore, it is of significant importance to developing electrolytes that are compatible with both high-voltage cathode and Li metal anode for practical LMBs.[7, 8]

Currently, various electrolyte engineering approaches, including salt/solvent optimization,[9, 10] additive screening[11, 12] and electrolyte concentration tuning,[13, 14] have been proposed to enhance their electrochemical stabilities. Among various electrolyte systems, ether-based electrolytes with excellent compatibility with Li metal hold great promise to practical LMBs. Nevertheless, ether solvents have inherently poor anodic stability (<4.0 V vs. Li/Li$^+$), thus have been excluded from high-voltage battery systems from the very beginning. Recently, ether-based high concentration electrolytes (HCEs) or local high concentration electrolytes (LHCEs) with high salt/solvent ratios have shown great potential with the enhanced anodic stability of Li$^+$-bounded ether solvent and the formation of inorganic-rich interphases due to their anion-dominated solvation structure.[14, 15] Outstanding electrochemical performances of high voltage LMBs (up to 4.5 V) have been demonstrated with ether-based LHCEs.[16] Nevertheless, typical concentrated ether electrolytes generally suffer from several inherent limitations. Firstly, the sluggish Li$^+$ transportation due to the featured intimate cation-anion coordination greatly increases cell polarization and undermines the rate performance.[17, 18] In addition, liable free ether solvent cannot be entirely eliminated due to the dynamic solvation/de-solvation process, which severely restricts the upper voltage limit of concentrated electrolytes. Recent studies have shown that introducing strong electron-withdrawing functional groups into the solvent

structure can improve their inherent oxidation stability.[19-22] Several ether molecules with difluoro or trifluoro functional groups have demonstrated enhanced high voltage stabilities for LMBs (under 4.3~4.4 V).[23, 24] Nevertheless, salt dissolution ability of the solvent would be compromised due to the existence of multi-fluorinated moieties at the vicinity of Li^+-coordination sites (e.g., oxygen atoms).

Here, to address the above dilemma for high-efficiency electrolyte design, we synthesized a unique monofluoro-ether solvent, 1,2-bis(2-fluoroethoxy) ethane (FDEE), with a single F substitution of only one β-H on each end. With the monofluorination strategy of ether solvent reported here for the first time, the charge density on ethereal oxygen atoms could be finely modulated to enable high oxidation stability and high salt solubility simultaneously. More importantly, a unique $Li^+\cdots F$-CH_2- interaction between Li^+ and FDEE is induced in the inner solvation sheath, which further enhances its Li^+-solvating ability and significantly increases the ionic conductivity with weakened anion coordination. Because of the robust and highly conductive interphases formed on both the Ni-rich cathode and the Li anode, the FDEE-based LHCE not only greatly improves the cycling stabilities of NMC811 cathodes under ultrahigh voltages (4.6 V and 4.7 V), but also enables an extremely high Li CE of 99.4%. Furthermore, extraordinary high-rate performances could be realized with FDEE in Li‖Li symmetric cells and Li‖NMC811 cells. This study provides a promising strategy of electrolyte design for fast-charging high energy density LMBs.

Results and discussion

Unique properties of FDEE and reduced Li^+-Anion coordination

FDEE was synthesized via a facial one-step substitution method using 1,2-bis(2-chloroethoxy)-ethyl ether (ClDEE) and potassium fluoride (KF) as the low-cost precursors (**Scheme S1** and **Table S1**), which suggests its potential for large-scale production. Nuclear magnetic resonance (NMR) spectra (^1H, ^{13}C and ^{19}F) confirm the successful synthesis of high purity FDEE (**Figure S1-3**). **Figure 1**a illustrates the molecular electrostatic potential (ESP) maps and theoretical oxidation potentials (E_{ox}) derived from density functional theory (DFT) calculations, which show significant decreases in the electron cloud density of oxygen atoms due to the electron-withdrawing effect of both Cl and F atoms.[22, 25] The increased theoretical

oxidation potentials also indicate their improved oxidation stabilities compared to the parent molecule DEE. Thanks to the high salt solubility with monofluorination, LHCEs were formulated with LiFSI as the single salt and TTE as the non-solvating diluent. To better illustrate the special role of the monofluoro group, three ether-based LHCEs were tested with molar ratios of electrolyte components as follows: LiFSI-DEE-TTE (1: 1.0: 3), LiFSI-ClDEE-TTE (1: 1.6: 3) and LiFSI-FDEE-TTE (1: 1.65: 3), respectively. Despite the varied Li$^+$-solvation ability of different ether molecules, the Li salt contents are close to their solubility limits in the three electrolytes for fair comparison. Linear sweep voltammetry (LSV) results also agree with the theoretical prediction (**Figure 1**e).
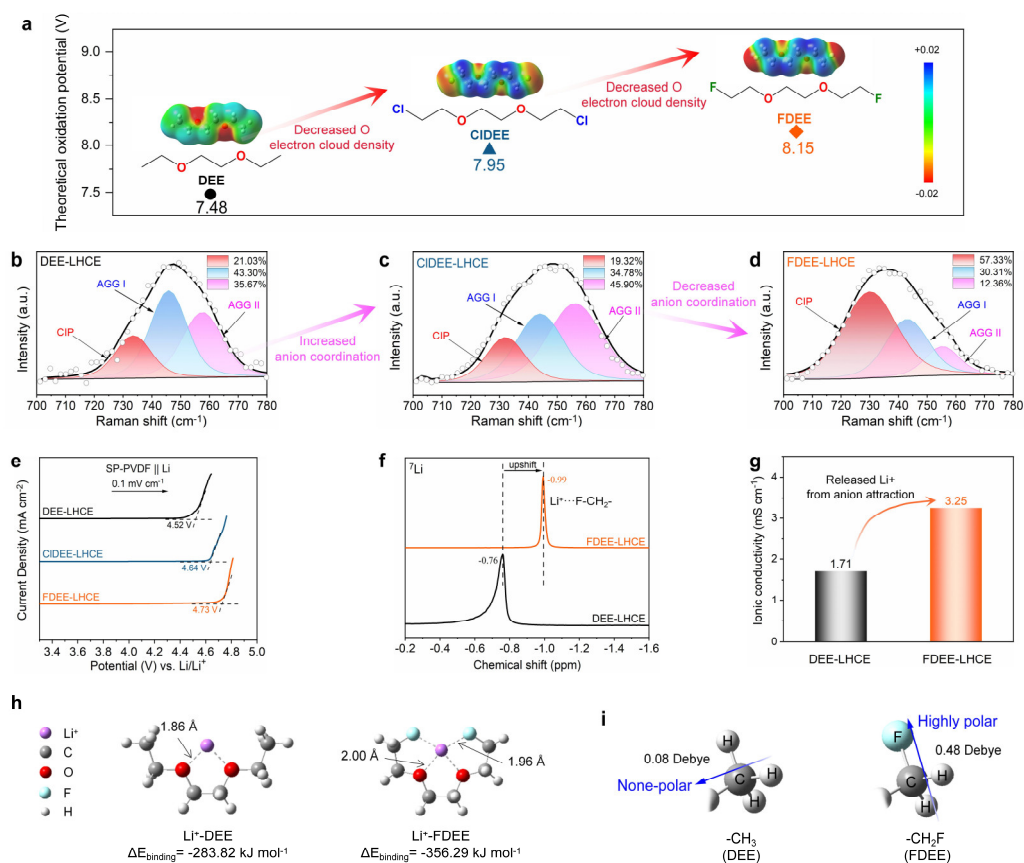
Figure 1. (a) The molecular electrostatic potential (ESP) maps and calculated theoretical oxidation potentials (E$_{ox}$) of DEE, ClDEE and FDEE. Raman spectra of (b) DEE-LHCE, (c) DEE-LHCE and (d) DEE-LHCE. (e) LSV measurements of the three ether-based LHCEs. (f) ^{7}Li-NMR spectra of DEE-LHCE and FDEE-LHCE. (g) Electrolyte ionic conductivity at 25 °C. (h) Binding energy of Li$^+$ between DEE and FDEE. (i) Dipole moments of -CH$_3$ (DEE) and -CH$_2$F (FDEE).

To study the influence of different substituents on the electrolyte solvation structure, Raman spectra of different electrolytes were collected (**Figure 1**b-d).[26-28] In DEE-LHCE, the high content of AGG (aggregate cluster) solvation structure indicates the strong coordination of anion with Li$^+$. This could be attributed to the high salt/solvent ratio and the steric effect of the ethoxy end groups, which decreases the Li$^+$-solvating ability of the ether solvent. Such strong anion coordination was found to be critical for enhancing the interfacial stability on the high-voltage cathode and the Li anode.[29] Higher contents of AGG, especially AGG-II (one FSI$^-$ coordinating to more than two Li$^+$) were observed in ClDEE-LHCE due to the electron-withdrawing effect of the Cl substitution. Nevertheless, such strong anion coordination would unavoidably decrease the ionic conductivity of the electrolyte and impede the battery rate performance. Surprisingly, a significantly lower content of AGG and a higher content of CIP (contact ion pair) were observed in FDEE-LHCE despite of the stronger electron-withdrawing effect of the F substitution , which suggests the unique ability of FDEE to reduce the anion coordination in the electrolyte solvation structure. This phenomenon is even more dramatic in dilute electrolytes due to excessive solvent presence (**Figure S4**), as evidenced by ^{17}O-NMR (**Figure S5**).[30] The stark difference for FDEE is likely due to the special Li$^+\cdots$F-CH$_2$- interaction between FDEE and Li$^+$, as suggested by the induced chemical shifts of ^{7}Li-NMR and ^{19}F-NMR (**Figure 1**f and **Figure S6-8**).[23, 24, 31] Such interaction apparently increases the solvating ability of FDEE (**Figure S9**) to reduce the anion coordination for more facial ionic conduction.[29, 32] As indicated in **Figure 1**g, the ionic conductivity of FDEE-LHCE (~3.25 mS cm^{-1}) is about twice of that in DEE-LHCE (~1.71 mS cm^{-1}).

As shown in **Figure 1**h, DFT calculations indicate stronger binding between Li$^+$ and FDEE than DEE, which agrees with the experimental results. Molecular dynamics (MD) simulation also shows the close proximity between Li$^+$ and the F atom on FDEE except for the common presence of FSI$^-$ in the inner solvation,[33] and strongly suggests the existence of Li$^+\cdots$F-CH$_2$- interactions (**Figure S10**). Moreover, it should be noted that the unique monofluorination strategy dramatically increases the dipole moment of the end group from 0.08 Debye (-CH$_3$) to 0.48 Debye (-CH$_2$F), which is also much higher than previously reported difluorine substitution of -CHF$_2$ and -CF$_3$ groups (**Figure S11**).[23, 24] In summary, the mono-fluorinated FDEE enhances

the oxidation stability and retains the high salt solubility of ether solvents. The high local polarity of -CH$_2$F enables peculiar Li$^+$···F-CH$_2$- interaction for reduced anion coordination and high ionic conductivity.

Ultrahigh-voltage LMB performance and the robust cathode-electrolyte interphase

To evaluate the high-voltage stability and fast-charging performance of the LHCEs based on different DEE derivatives, LMBs with highly active polycrystalline (PC) NMC811 cathodes (with a moderately high areal loading of 1.7 mAh cm^{-2}) were tested. As shown in **Figures 2**a and c-e, DEE-LHCE shows overcharging in the first cycle below the 4.6 V cut-off voltage. The rich reactive sites on PC-NMC811 also induce continuous side reactions with ClDEE-LHCE during cycling. In sharp contrast, the cell using FDEE-LHCE exhibits a greatly improved cycling stability under 4.6 V, with a high capacity retention (>80%) after 200 cycles on PC-NMC811 at C/3. Single crystalline (SC) NMC811 cathodes were also tested to better probe the inherent stability of different electrolytes on the NMC811 surface without the interference of secondary particle cracking. As shown in **Figure 2**f and **S12-13,** excellent cycling performance at both 4.6 V (93.7% capacity after 250 cycles) and 4.7 V (93.7% capacity after 150 cycles) are realized. To the best of our knowledge, this is the first time for LMBs to achieve such high-voltage cycling performances with ether-based electrolytes. Compared to DEE-LHCE and ClDEE-LHCE, the outstanding high-voltage stability of FDEE-LHCE should be attributed to the superior anti-oxidation capability with monofluoro substituents and the favorable solvation structure. As shown in **Figure S14**, the leakage current of the NMC811 cell using FDEE-LHCE is also the smallest among the three LHCEs.[9, 34] Both cycled full cells and symmetric cells (NCM811‖NCM811 and Li‖Li) using FDEE-LHCE show dramatically decreased interfacial impedances, highlighting the highly favorable interfacial charge transfer processes on both the cathode and the Li anode (**Figures S15-16**). Even under practical conditions with thin Li anode and lean electrolyte or anode-free setup, the cells with FDEE-LHCE can still achieve good cycling stabilities (**Figure S17**). Because of the favorable ionic conduction in the FDEE-LHCE and at the electrode/electrolyte interfaces, excellent high-rate performance of LMBs could be demonstrated (**Figure 2**b).[34, 35] FDEE-LHCE has achieved unprecedented cell performance compared to the reported advanced electrolytes applied in NMC-based LMBs under high

voltage (4.6 V and 4.7 V) and fast-charging conditions (up to 5.1 mA cm^{-2}), as shown in **Figure 2g, Figure S18-S21** and **Table S2**.
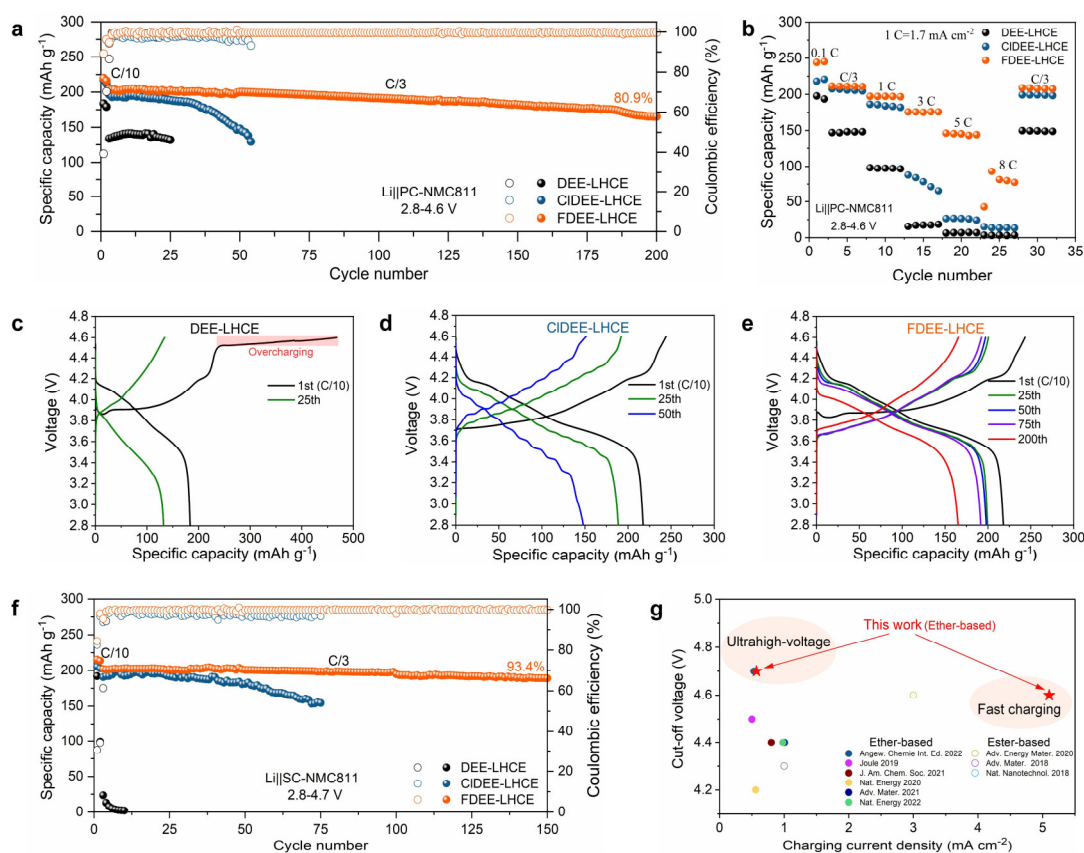
Figure 2. Electrochemical performances of Li||NMC811 cells. (a) Specific capacity and Coulombic efficiency of 4.6 V PC-NMC811 cells under C/3. (b) Rate performance of 4.6 V PC-NMC811 cells in different electrolytes. Voltage profiles of the 4.6 V PC-NMC811 cells under C/3 using (c) DEE-LHCE, (d) ClDEE-LHCE and (e) FDEE-LHCE. (f) 4.7 V SC-NMC811 cells using different electrolytes under C/3. (g) Comparison of charging current density and cut-off voltage used for FDEE-LHCE and advanced electrolytes applied in NMC-based LMBs.

Scanning electron microscope (SEM) was employed to characterize the morphology of the cathodes before and after cycling. As shown in **Figure 3**a, the cycled cathode in DEE-LHCE is completely covered with deposits due to the severe decomposition of DEE under 4.6 V. Due to the electrolyte penetration into the grain boundary of primary particles and the continuous growth of CEI on newly exposed surfaces during cycling, the PC-NMC811 particle gradually cracks in ClDEE-LHCE.[36] In sharp contrast, the cathode cycled in FDEE-LHCE retains intact morphology. The effect of different electrolytes on the cathode stability is also supported by the amounts of transition metal ions (Ni, Co and Mn) deposited on the LMA as detected by

ICP-MS, which shows that the dissolution of transition metal from the cathode is effectively inhibited during high voltage cycling in FDEE-LHCE (**Figure S22**).
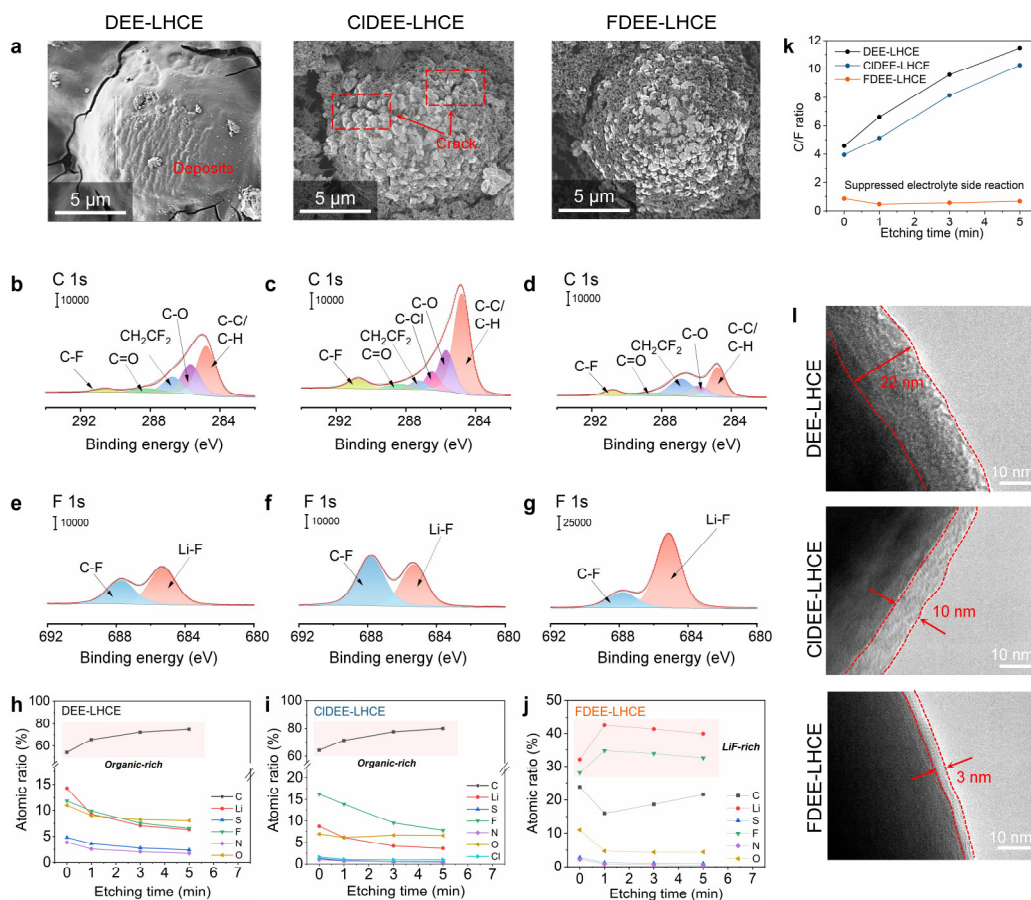
Figure 3. (a) SEM images, C 1s and F 1s XPS spectra (profiling depth=0) of the cathodes under 4.6 V after 50 cycles in (b,e) DEE-LHCE, (c,f) ClDEE-LHCE and (d,g) FDEE-LHCE. The atomic ratio of CEIs on the cathodes after 50 cycles in (h) DEE-LHCE, (i) ClDEE-LHCE and (j) FDEE-LHCE by XPS depth profiling. (k) The C/F ratio of the cycled cathodes . (l) TEM images of the cycled cathodes

To further investigate the stabilization mechanism of high-voltage PC-NMC811 cathodes, the compositions of CEI films were analyzed by X-ray photoelectron spectroscopy (XPS) along with depth profiling. In the C 1s spectrum (**Figure 3** and **Figure S23**), fewer organic species including C-C/C-H, C-O and C=O and lower atomic ratios of C were observed during depth profiling on the cathode cycled in FDEE-LHCE which suggests less solvent-related side reactions. In addition, the strongest inorganic Li-F signal (685.7 eV) in the F 1s spectrum (**Figure 3**e-g and **Figure S24**) and the extremely low C/F ratio throughout the depth profiling

are detected on the cycled cathode with FDEE-LHCE, which demonstrates that the LiF-rich CEI formed in FDEE-LHCE effectively inhibits further solvent oxidation and protects the NMC811 cathode (**Figure 3**h-k).[22, 37, 38] A thinner and more uniform CEI of only 3 nm was observed in FDEE-LHCE by transmission electron microscopy (TEM), compared to the other electrolytes (**Figure 3**l). Given the fact that all the three LHCEs contain similar ratios of identical fluorinated species (LiFSI and TTE), it is very surprising to find the significant enrichment of LiF species with the FDEE-based electrolyte, where the CIP structure with low FSI^- coordination in the inner solvation sheath is in dominance. In addition, the relative ratios of F element to S, N and O in the CEI are dramatically higher in FDEE-LHCE than those in DEE-LHCE and ClDEE-LHCE (**Figure S25**). Therefore, it is most likely that FDEE molecules have a prominent contribution in the formation process of LiF on the NMC811 particle surface. The highly polar $-CH_2F$ groups, which have strong $Li^+ \cdots F-CH_2-$ interactions in the solvation complex, could be catalytically cleaved by the active sites on the cathode surface to deposit LiF for immediate passivation. This process may proceed before the decomposition of FSI^- induced by intermediators from interfacial reactions.[39, 40] As a result, a much thinner CEI was constructed by FDEE-LHCE, while FSI^--derivated CEIs in DEE-LHCE and ClDEE-LHCE are thicker with higher contents of SO_x and NO_x species (**Figure S26, 27**).

High-efficiency Li metal anode and the anode-electrolyte Interphase

Figure 4a shows the Li CE results in the three LHCEs using the Aurbach method.[41] Both DEE-LHCE and ClDEE-LHCE display similar CEs of ~99.2%, while FDEE-LHCE shows a higher value of 99.4%. For the full stripping test shown in **Figure 4**b, the cells using the three LHCEs all show high CEs within 100 cycles, which is associated with the stabilization of Li metal by the high LiFSI/solvent ratios in LHCEs.[42-44] The Li depositions in different electrolytes also show particle-like morphologies without Li dendrites (**Figure 4**c-e). However, the cell in FDEE-LHCE could cycle steadily for more than 350 cycles and reach a high average Li CE of 99.4%. As demonstrated in (**Figures 4**f,g and **Figure S28**), it is surprising that the Li CE in 1M LiFSI/FDEE rises to 99% within 3 cycles. These results indicate the unique ability of FDEE to protect Li metal compared to the DEE parent molecule and the chlorinated ClDEE. Furthermore, as shown in **Figure 4**h-j and **Figure S29, 30**, FDEE-LHCE and FDEE-based dilute electrolytes

exhibit a constantly small cell voltage hysteresis during long-term cycling in Li∥Cu and Li∥Li cells.[9, 45] Even under an ultrahigh current density of 10 mA cm⁻², the Li∥Li cell with FDEE-LHCE could operate very stably for more than 800 h with an overpotential about 50 mV (**Figure 4**l), which could be attributed to its highest exchange current density, the lowest Li⁺ diffusion resistance as well as the smallest activation energy (E_{al}) (**Figure 4**k and **Figure S31**).[30, 46, 47]
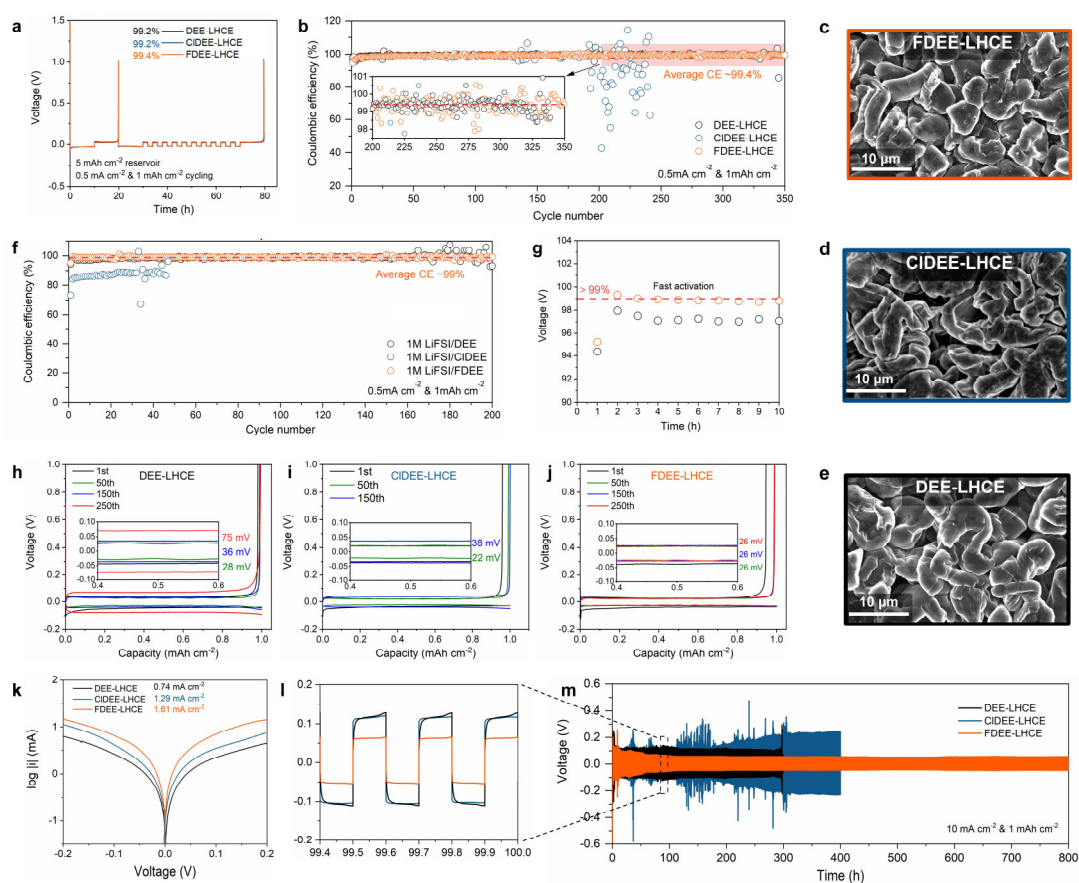
Figure 4. (a) Li CE tests using the Aurbach method in different electrolytes. (b) Cycling stability of Li CEs in Li∥Cu cells using different electrolytes. (c-e) The top-section views of SEM images (deposited 4 mAh cm⁻² Li films under 0.5 mA cm⁻²) in different electrolytes. (f,g) Cycling stability of Li CEs in Li∥Cu cells using different dilute electrolytes. (h-j) Voltage profiles of Li∥Cu cells. (k) Exchange current density test Li∥Li symmetric cells after 10 cycles under 0.5 mA cm⁻². (l,m) Cycling stability of Li∥Li symmetric cells cycling under 10 mA cm⁻².

To further understand the reaction mechanism of FDEE-LHCE on Li anode, SEI films formed on Li anode from cycled Li∥PC-NMC811 cells were characterized by XPS depth

profiling. Similar signals (Li-F, N-SO$_x$, SO$_x$ and S$_n^{2-}$) can be found on Li anodes using the three LHCEs due to the preferred decomposition of FSI$^-$ in LHCEs (**Figure S32-35**). However, the accumulation of organic components on the Li anode is apparently less in FDEE-LHCE compared to that in DEE-LHCE and ClDEE-LHCE. The atomic ratio results (**Figure S36**) show that the Li anode surface with FDEE-LHCE exhibits high Li/O/F content and maintains a stable ratio at different profiling depths, indicating that the SEI film has a high uniformity at different depths. Obviously lower signals of C-O (531 eV, O 1s) were found on the Li anode in FDEE-LHCE throughout depth profiling, which may suggest the enhanced Li metal protection for the electrolyte[48]. Another possibility could be the less amount of solvent decomposition product crossover from the high-voltage cathode, as indicated by the electrolyte color change after cycling (**Figure S37**). In addition, it was noticed that the Li anode cycled in FDEE-LHCE has higher signal intensities for Li$_2$O and LiN$_x$, which are favorable for Li$^+$ transport in the SEI (**Figure S33 and S35**).[49,50] It is likely that the Li$^+$ solvation complexes composed of FDEE and FSI$^-$ can decompose simultaneously on the Li metal anode to derive a uniform SEI film that riches in various inorganic and organic species,[33] which helps to protect the Li metal anode and promote Li$^+$ transport. From the top-section and cross-section SEM images of cycled Li anodes, FDEE-LHCE also induces a smoother surface morphology and a thinner surface corrosion layer than the other electrolytes (**Figure S38**).

Conclusion

In summary, we designed and synthesized a new monofluorinated ether (FDEE), which successfully addressed the inherent issues of sluggish ionic conduction and limited oxidation stability of ether-based concentrated electrolytes. The highly polar monofluoro -CH$_2$F group induces a strong interaction with Li$^+$, which greatly enhances its Li$^+$-solvating ability and reduce anion coordination for fast ion transportation. The FDEE-based LHCE shows very rare combination of merits in terms of high ionic conductivity (nearly double that of DEE-LHCE), fast-charging (10 mA cm^{-2}), high Li CE (99.4%), ultrahigh-voltage stability (4.6 V and 4.7 V) and non-flammability (**Video S1-S4**). Such electrochemical performances of LMB marks a major step in the development of electrolytes, especially for concentrated electrolyte systems. This study provides a new electrolyte design approach for LMBs and highlights the critical role of molecular design to meet the demanding challenges of practical high energy density LMBs.

Experimental Section

Materials: 1,2-diethoxyethane (DEE) and 1,1,2,2-Tetrafluoroethyl-2,2,3,3-tetrafluoropropylether (TTE) were purchased from Meryer and Shang Fluoro Technology Co., Ltd., respectively. Tetraethylene glycol (TEG) was ordered from Macklin, while 1,2-Bis(2-chloroethoxy) ethane (ClDEE) and potassium fluoride (KF) were provided by Aladdin. To avoid the influence of trace water, all the above solvents were dried with molecular sieve for more than 3 days before use. Thick Li metal chips (thickness is 450 μm and radius is 15.6 mm) and thin Li foil (thickness is 50 μm and radius is 15.6 mm) were purchased from China Energy Lithium Co., Ltd. LiFSI (99%) was supplied by Nippon Shokubai (Japan) and dried under vacuum at 100 °C for 24 hours before use. Poly-crystal and single-crystal NMC811 powers were purchased from Hunan ShanShan New Material Co., Ltd. and Shenzhen Kejing materials technology Co., Ltd, respectively. Both poly-crystal and single-crystal NMC811 slurries composed of NMC811, polyvinylidene fluoride (PVDF) in N-methyl-2-pyrrolidone (NMP) and super P Li in a ratio of 80%:10%:10% (in weight) were coated on the aluminum foil for low loading NMC811. The high loading of NMC811 was prepared in the same way, except that the above ratio was 90%:5%:5%. The obtained cathode chips were dried at 110 °C under vacuum before use. Radius of cathode pieces 12 mm. The low and high loading of NMC811 active material were 10 ± 0.5 mg cm^{-2} and 20 ± 0.5 mg cm^{-2}, respectively. High loading cathodes were used for the cells under practical condition and anode-free, while low loading cathodes were used for the rest of tests.

Synthesis of 1,2-bis(2-fluoroethoxy) ethane (FDEE): ClDEE and KF were mixed at a molar ratio of 1:4, and the reaction solvent TEG was added (0.1 mol KF corresponds to 25 mL of TEG), and then the mixture was magnetically stirred at 180 °C for 8.5 h. After the reaction, the liquid was filtered and extracted with anhydrous ether. The obtained extraction supernatant was rotary evaporated to remove the ether. In order to gain high purity sample, crude sample was further vacuum distilled to obtain a pale yellow clear liquid (reaction yield: 23%). The final product was transferred to the argon-filled glove box (H$_2$O<0.1 ppm, O$_2$<0.1 ppm) and dried with molecular sieves for more than three days before use. Nuclear magnetic resonance (NMR) was used to characterize the synthesized sample. ^{1}H-NMR (400 MHz, CDCl$_3$, δ/ppm): 4.57 (dt, 4H, J=47.7 Hz, J=4.15 Hz), 3.78 (t, 2H, J=4.15 Hz), 3.65-3.76 (m, 6H). ^{13}C-NMR (400 MHz,

CDCl$_3$, δ/ppm): 83.25 (d, 2C, J=169 Hz), 70.95 (s, 2C), 70.57 (d, 2C, J=19.7 Hz). ^{19}F-NMR (400 MHz, CDCl$_3$, δ/ppm): -223.97 (tt, 2F, J=45.8 Hz, J=27.8 Hz).

Electrolyte preparations: All electrolyte preparations were carried out in the argon-filled glove box (H$_2$O<0.1 ppm, O$_2$<0.1 ppm). 1 mol LiFSI was dissolved in 1 mL DEE or ClDEE or FDEE to obtain 1 M LiFSI/DEE or 1 M LiFSI/ClDEE or 1 M LiFSI/FDEE, respectively. LHCE preparation with LiFSI: DEE or ClDEE or FDEE: TTE=1:1.0 or 1.60 or 1.65: 3 was mixed in molar ratio to obtain DEE-LHCE or ClDEE-LHCE or FDEE-LHCE, respectively.

Electrochemical measurements: All CR2032 coin cells (Guangdong Canrd New Energy Technology) using Celgard 2500 separator were assembled in the argon-fill glovebox (H$_2$O<0.1 ppm, O$_2$<0.1 ppm). The electrochemical cycling measurements were carried out on Land CT2001A (Wuhan, China) and Neware (Shenzhen, China) at room temperature (25 ℃). Li‖Cu half cells, 1.0 mAh cm^{-2} Li metal was electrodeposited at 0.5 mA cm^{-2} onto the bare Cu substrate and then stripped until a cut-off voltage of 1 V in each cycle. For the Aurbach CE test, the standard method is as follows: 1) Quantitative Li (5 mAh cm^{-2}) is electrochemically deposited on the surface of the copper foil at 0.5 mA cm^{-2} and stripping to 1 V; 2) Li (5 mA h cm^{-2}) is deposited on the copper foil again under 0.5 mA cm^{-2}; 3) repeatedly deposit/strip Li of 1 mAh cm^{-2} under 0.5 mA cm^{-2}, 2 mA cm^{-2}, 5 mA cm^{-2} or 10 mA cm^{-2} for 10 cycles; 4) strip all Li to 1 V. Li‖Li symmetric cells were conducted with 1.0 mAh cm^{-2} plating/stripping in each cycle at a current density of 0.5 mA cm^{-2} or 10 mA cm^{-2}. Li‖NMC811 cells were cycled at C/10 rates (1C=180 mAh g^{-1}) for two formation cycles, and cycled at 1/3C, 1 C, 2 C, 3 C and 5C for the following cycled in the voltage range of 2.8-4.5 V, 2.8-4.6 V or 2.8-4.7 V. Electrochemical impedance spectroscopy (EIS) were measured in a frequency range from 100 mHz to 1 MHz with an AC amplitude of 5 mV on a Solartron frequency analyzer for cycled Li‖PC-NMC811, and from 10 mHz to 1 MHz with an AC amplitude of 5 mV for NMC811‖NMC811 symmetric cells, and from 100 mHz to 100 kHz with an AC amplitude of 10 mV for Li‖Li symmetric cells, and from 10 mHz to 100 kHz with an AC amplitude of 10 mV for Li‖Li symmetric cells in activation energy test. The amount of electrolyte in each cell is 75 μL, except for 20 μL used in cell under practical condition.

Physical characterizations: The cycled cells were disassembled in the glove box. The collected electrodes were rinsed by DME for at least three times to remove the remaining

electrolytes and dried in vacuum. ESCALAB 250Xi model X-ray photoelectron spectroscopy (XPS) was employed to test the surface compositions of both NMC811 cathodes and the Li anodes. A Gemini SEM 500 microscope was used to characterize electrode samples. TEM (Talos F200X) was applied to observe the thickness and morphology of CEI films, and the cathode samples were dispersed in ultrasonic in N, N-Dimethylacetamide before testing. For ICP-MS measurements, the cycled Li anodes were completely dissolved in 5 wt% HNO_3, and then the solution volumes were fixed with a 25 ml volumetric flask. NMR was used to study the solvation structure of electrolytes, where ^{19}F, ^{7}Li and ^{17}O were performed by 400 MHz Brooke, 600 MHz Brooke and 600 MHz Varian (solid-state NMR), respectively.

Theoretical calculations: Quantum chemistry calculations were first performed to optimize molecular geometries of DEE, ClDEE, FDEE, and TTE molecules using the Gaussian 16 package at B3LYP/6-311+G(d,p) level of theory.[1] The atomic partial charges on these solvent molecules were computed by fitting to the molecular electrostatic potential at atomic centers with the Møller-Plesset second-order perturbation method and the correlation-consistent polarized valence cc-pVTZ(-f) basis set. The atomistic force field parameters for all ions and molecules are described by the OPLS-AA format and are taken from previous work.[2] The cross-interaction parameters between different atom types are obtained from the Lorentz-Berthelot combination rule. The theoretical oxidation potential (E_{ox}) and binding energy ($\triangle E_{binding}$) were calculated by the following formulas:

$$E_{ox}(Li/Li^+) = [G(M^+) - G(M)]/F - 1.4 \text{ V} \tag{1}$$

$$\triangle E_{binding}(G-Li^+) = E(G-Li^+) - E(G) - E(Li^+) \tag{2}$$

where $G(M)$ and $G(M^+)$ are the Gibbs free energy of the species M and its oxidized form M^+ at 298.15 K, respectively, while F is the Faraday constant.

Atomistic simulations were performed using GROMACS package with cubic periodic boundary conditions.[3] The equations for the motion of all atoms were integrated using a classic Verlet leapfrog integration algorithm with a time step of 1.0 fs. A cutoff radius of 1.6 nm was set for short-range van der Waals interactions and real-space electrostatic interactions. The particle-mesh Ewald (PME) summation method with an interpolation order of 5 and a Fourier grid spacing of 0.20 nm was employed to handle long range electrostatic interactions in reciprocal space. All simulation systems were first energetically minimized using a steepest

descent algorithm, and thereafter annealed gradually from 600 K to room temperature (300 K) within 10 ns. All annealed simulation systems were equilibrated in an isothermal-isobaric (NPT) ensemble for 20 ns of physical time maintained using a Nosé-Hoover thermostat and a Parrinello-Rahman barostat with time coupling constants of 0.4 and 0.2 ps, respectively, to control the temperature at 300 K and the pressure at 1 atm. Atomistic simulations were further performed in a canonical ensemble (NVT) for 50 ns, and simulation trajectories were recorded at an interval of 100 fs for further structural and dynamical analysis.

References
(1)   Liu, J.; Bao, Z.; Cui, Y.; Dufek, E. J.; Goodenough, J. B.; Khalifah, P.; Li, Q.; Liaw, B. Y.; Liu, P.; Manthiram, A.; Meng, Y. S.; Subramanian, V. R.; Toney, M. F.; Viswanathan, V. V.; Whittingham, M. S.; Xiao, J.; Xu, W.; Yang, J.; Yang, X.-Q.; Zhang, J.-G., Pathways for practical high-energy long-cycling lithium metal batteries. *Nat. Energy* **2019,** *4* (3), 180-186.
(2)   Xu, W.; Wang, J.; Ding, F.; Chen, X.; Nasybulin, E.; Zhang, Y.; Zhang, J.-G., Lithium metal anodes for rechargeable batteries. *Energy Environ. Sci.* **2014,** *7* (2), 513-537.
(3)   Zhang, J. G.; Xu, W.; Xiao, J.; Cao, X.; Liu, J., Lithium Metal Anodes with Nonaqueous Electrolytes. *Chem. Rev.* **2020,** *120* (24), 13312-13348.
(4)   Myung, S.-T.; Maglia, F.; Park, K.-J.; Yoon, C. S.; Lamp, P.; Kim, S.-J.; Sun, Y.-K., Nickel-Rich Layered Cathode Materials for Automotive Lithium-Ion Batteries: Achievements and Perspectives. *ACS Energy Lett.* **2016,** *2* (1), 196-223.
(5)   Li, W.; Erickson, E. M.; Manthiram, A., High-nickel layered oxide cathodes for lithium-based automotive batteries. *Nat. Energy* **2020,** *5* (1), 26-34.
(6)   Maleki Kheimeh Sari, H.; Li, X., Controllable Cathode-Electrolyte Interface of Li[$Ni_{0.8}Co_{0.1}Mn_{0.1}$]O_2 for Lithium Ion Batteries: A Review. *Adv. Energy Mater.* **2019,** *9* (39), 1901597.
(7)   Xu, K., Nonaqueous Liquid Electrolytes for Lithium-Based Rechargeable Batteries. *Chem. Rev.* **2004,** (104), 4303-4417.
(8)   Xu, K., Electrolytes and interphases in Li-ion batteries and beyond. *Chem. Rev.* **2014,** *114*

(23), 11503-11618.

(9) Xue, W.; Huang, M.; Li, Y.; Zhu, Y. G.; Gao, R.; Xiao, X.; Zhang, W.; Li, S.; Xu, G.; Yu, Y.; Li, P.; Lopez, J.; Yu, D.; Dong, Y.; Fan, W.; Shi, Z.; Xiong, R.; Sun, C.-J.; Hwang, I.; Lee, W.-K.; Shao-Horn, Y.; Johnson, J. A.; Li, J., Ultra-high-voltage Ni-rich layered cathodes in practical Li metal batteries enabled by a sulfonamide-based electrolyte. *Nat. Energy* **2021,** *6* (5), 495-505.

(10) Li, L.; Xu, G.; Zhang, S.; Dong, S.; Wang, S.; Cui, Z.; Du, X.; Wang, C.; Xie, B.; Du, J.; Zhou, X.; Cui, G., Highly Fluorinated Al-Centered Lithium Salt Boosting the Interfacial Compatibility of Li-Metal Batteries. *ACS Energy Lett.* **2022,** *7* (2), 591-598.

(11) Ruan, D.; Chen, M.; Wen, X.; Li, S.; Zhou, X.; Che, Y.; Chen, J.; Xiang, W.; Li, S.; Wang, H.; Liu, X.; Li, W., In situ constructing a stable interface film on high-voltage LiCoO2 cathode via a novel electrolyte additive. *Nano Energy* **2021,** *90*, 106535.

(12) Zhang, Y.; Wu, Y.; Li, H.; Chen, J.; Lei, D.; Wang, C., A dual-function liquid electrolyte additive for high-energy non-aqueous lithium metal batteries. *Nat. Commun.* **2022,** *13* (1), 1297.

(13) Jiao, S.; Ren, X.; Cao, R.; Engelhard, M. H.; Liu, Y.; Hu, D.; Mei, D.; Zheng, J.; Zhao, W.; Li, Q.; Liu, N.; Adams, B. D.; Ma, C.; Liu, J.; Zhang, J.-G.; Xu, W., Stable cycling of high-voltage lithium metal batteries in ether electrolytes. *Nat. Energy* **2018,** *3* (9), 739-746.

(14) Wang, J.; Yamada, Y.; Sodeyama, K.; Chiang, C. H.; Tateyama, Y.; Yamada, A., Superconcentrated electrolytes for a high-voltage lithium-ion battery. *Nat. Commun.* **2016,** *7*, 12032.

(15) Ren, X.; Zou, L.; Jiao, S.; Mei, D.; Engelhard, M. H.; Li, Q.; Lee, H.; Niu, C.; Adams, B. D.; Wang, C.; Liu, J.; Zhang, J.-G.; Xu, W., High-Concentration Ether Electrolytes for Stable High-Voltage Lithium Metal Batteries. *ACS Energy Lett.* **2019,** *4* (4), 896-902.

(16) Ren, X.; Zhang, X.; Shadike, Z.; Zou, L.; Jia, H.; Cao, X.; Engelhard, M. H.; Matthews, B. E.; Wang, C.; Arey, B. W.; Yang, X. Q.; Liu, J.; Zhang, J. G.; Xu, W., Designing Advanced In Situ Electrode/Electrolyte Interphases for Wide Temperature Operation of 4.5 V Li‖LiCoO2 Batteries. *Adv. Mater.* **2020,** *32* (49), e2004898.

(17) Cao, X.; Jia, H.; Xu, W.; Zhang, J.-G., Review-Localized High-Concentration Electrolytes for Lithium Batteries. *J. Electrochem. Soc.* **2021,** *168* (1), 010522.

(18) Yamada, Y.; Wang, J.; Ko, S.; Watanabe, E.; Yamada, A., Advances and issues in developing salt-concentrated battery electrolytes. *Nat. Energy* **2019,** *4* (4), 269-280.

(19) Su, C.-C.; He, M.; Shi, J.; Amine, R.; Yu, Z.; Cheng, L.; Guo, J.; Amine, K., Principle in developing novel fluorinated sulfone electrolyte for high voltage lithium-ion batteries. *Energy Environ. Sci.* **2021,** *14* (5), 3029-3034.

(20) Zhou, T.; Zhao, Y.; El Kazzi, M.; Choi, J. W.; Coskun, A., Integrated Ring-Chain Design of a New Fluorinated Ether Solvent for High-Voltage Lithium-Metal Batteries. *Angew. Chem. Int. Ed.* **2022,** *61* (19), e202115884.

(21) Zhao, Y.; Zhou, T.; Ashirov, T.; Kazzi, M. E.; Cancellieri, C.; Jeurgens, L. P. H.; Choi, J. W.; Coskun, A., Fluorinated ether electrolyte with controlled solvation structure for high voltage lithium metal batteries. *Nat. Commun.* **2022,** *13* (1), 2575.

(22) Tan, L.; Chen, S.; Chen, Y.; Fan, J.; Ruan, D.; Nian, Q.; Chen, L.; Jiao, S.; Ren, X., Intrinsic Nonflammable Ether Electrolytes for Ultrahigh-Voltage Lithium Metal Batteries Enabled by Chlorine Functionality. *Angew. Chem. Int. Ed.* **2022,** e202203693.

(23) Yu, Z.; Wang, H.; Kong, X.; Huang, W.; Tsao, Y.; Mackanic, D. G.; Wang, K.; Wang, X.;

Huang, W.; Choudhury, S.; Zheng, Y.; Amanchukwu, C. V.; Hung, S. T.; Ma, Y.; Lomeli, E. G.; Qin, J.; Cui, Y.; Bao, Z., Molecular design for electrolyte solvents enabling energy-dense and long-cycling lithium metal batteries. *Nat. Energy* **2020,** *5* (7), 526-533.

(24) Z. Yu, P. E. R., Z. Zhang, Z. Huang, H. Celik, S. T. Oyakhire, Y. Chen, X. Kong, S. C. Kim, X. Xiao, H. Wang, Y. Zheng, G. A. Kamat, M. S. Kim, S. F. Bent, J. Qin, Y. Cui, Z. Bao, Rational solvent molecule tuning for highperformance lithium metal battery electrolytes. *Nat. Energy* **2022,** (7), 94-106.

(25) Zhang, Z.; Hu, L.; Wu, H.; Weng, W.; Koh, M.; Redfern, P. C.; Curtiss, L. A.; Amine, K., Fluorinated electrolytes for 5 V lithium-ion battery chemistry. *Energy Environ. Sci.* **2013,** *6* (6), 1806-1810.

(26) Li, T.; Zhang, X. Q.; Yao, N.; Yao, Y. X.; Hou, L. P.; Chen, X.; Zhou, M. Y.; Huang, J. Q.; Zhang, Q., Stable Anion-Derived Solid Electrolyte Interphase in Lithium Metal Batteries. *Angew. Chem. Int. Ed.* **2021,** *60* (42), 22683-22687.

(27) Pham, T. D.; Lee, K. K., Simultaneous Stabilization of the Solid/Cathode Electrolyte Interface in Lithium Metal Batteries by a New Weakly Solvating Electrolyte. *Small* **2021,** *17* (20), 2100133.

(28) Pham, T. D.; Bin Faheem, A.; Kim, J.; Oh, H. M.; Lee, K. K., Practical High-Voltage Lithium Metal Batteries Enabled by Tuning the Solvation Structure in Weakly Solvating Electrolyte. *Small* **2022,** e2107492.

(29) Chen, Y.; Yu, Z.; Rudnicki, P.; Gong, H.; Huang, Z.; Kim, S. C.; Lai, J. C.; Kong, X.; Qin, J.; Cui, Y.; Bao, Z., Steric Effect Tuned Ion Solvation Enabling Stable Cycling of High-Voltage Lithium Metal Battery. *J. Am. Chem. Soc.* **2021,** *143* (44), 18703-18713.

(30) Yao, Y. X.; Chen, X.; Yan, C.; Zhang, X. Q.; Cai, W. L.; Huang, J. Q.; Zhang, Q., Regulating Interfacial Chemistry in Lithium-Ion Batteries by a Weakly Solvating Electrolyte. *Angew. Chem. Int. Ed.* **2021,** *60* (8), 4090-4097.

(31) Kim, S. C.; Kong, X.; Vila, R. A.; Huang, W.; Chen, Y.; Boyle, D. T.; Yu, Z.; Wang, H.; Bao, Z.; Qin, J.; Cui, Y., Potentiometric Measurement to Probe Solvation Energy and Its Correlation to Lithium Battery Cyclability. *J. Am. Chem. Soc.* **2021,** *143* (27), 10301-10308.

(32) Su, C.-C.; He, M.; Shi, J.; Amine, R.; Zhang, J.; Guo, J.; Amine, K., Superior long-term cycling of high-voltage lithium-ion batteries enabled by single-solvent electrolyte. *Nano Energy* **2021,** *89*, 106299.

(33) Ren, X.; Gao, P.; Zou, L.; Jiao, S.; Cao, X.; Zhang, X.; Jia, H.; Engelhard, M. H.; Matthews, B. E.; Wu, H.; Lee, H.; Niu, C.; Wang, C.; Arey, B. W.; Xiao, J.; Liu, J.; Zhang, J. G.; Xu, W., Role of inner solvation sheath within salt-solvent complexes in tailoring electrode/electrolyte interphases for lithium metal batteries. *Proc. Natl. Acad. Sci. U.S.A.* **2020,** *117* (46), 28603-28613.

(34) Su, C.-C.; He, M.; Amine, R.; Chen, Z.; Sahore, R.; Dietz Rago, N.; Amine, K., Cyclic carbonate for highly stable cycling of high voltage lithium metal batteries. *Energy Stor. Mater.* **2019,** *17*, 284-292.

(35) Gao, N.; Kim, S.; Chinnam, P.; Dufek, E. J.; Colclasure, A. M.; Jansen, A.; Son, S.-B.; Bloom, I.; Dunlop, A.; Trask, S.; Gering, K. L., Methodologies for Design, Characterization and Testing of Electrolytes that Enable Extreme Fast Charging of Lithium-ion Cells. *Energy Stor. Mater.* **2022,** *44*, 296-312.

(36) Tian, C.; Lin, F.; Doeff, M. M., Electrochemical Characteristics of Layered Transition

Metal Oxide Cathode Materials for Lithium Ion Batteries: Surface, Bulk Behavior, and Thermal Properties. *Acc. Chem. Res.* **2018,** *51* (1), 89-96.

(37) Wu, F.; Fang, S.; Kuenzel, M.; Mullaliu, A.; Kim, J.-K.; Gao, X.; Diemant, T.; Kim, G.-T.; Passerini, S., Dual-anion ionic liquid electrolyte enables stable Ni-rich cathodes in lithium-metal batteries. *Joule* **2021,** *5* (8), 2177-2194.

(38) Nian, Q.; Zhu, W.; Zheng, S.; Chen, S.; Xiong, B. Q.; Wang, Z.; Wu, X.; Tao, Z.; Ren, X., An Overcrowded Water-Ion Solvation Structure for a Robust Anode Interphase in Aqueous Lithium-Ion Batteries. *ACS Appl. Mater. Interfaces* **2021,** *13* (43), 51048-51056.

(39) Fan, X.; Chen, L.; Borodin, O.; Ji, X.; Chen, J.; Hou, S.; Deng, T.; Zheng, J.; Yang, C.; Liou, S. C.; Amine, K.; Xu, K.; Wang, C., Non-flammable electrolyte enables Li-metal batteries with aggressive cathode chemistries. *Nat. Nanotechnol.* **2018,** *13* (8), 715-722.

(40) Xue, W.; Shi, Z.; Huang, M.; Feng, S.; Wang, C.; Wang, F.; Lopez, J.; Qiao, B.; Xu, G.; Zhang, W.; Dong, Y.; Gao, R.; Shao-Horn, Y.; Johnson, J. A.; Li, J., FSI-inspired solvent and "full fluorosulfonyl" electrolyte for 4 V class lithium-metal batteries. *Energy Environ. Sci.* **2020,** *13* (1), 212-220.

(41) Adams, B. D.; Zheng, J.; Ren, X.; Xu, W.; Zhang, J. G., Accurate Determination of Coulombic Efficiency for Lithium Metal Anodes and Lithium Metal Batteries. *Adv. Energy Mater.* **2017,** *8* (7), 1702097.

(42) Chen, S.; Zheng, J.; Mei, D.; Han, K. S.; Engelhard, M. H.; Zhao, W.; Xu, W.; Liu, J.; Zhang, J. G., High-Voltage Lithium-Metal Batteries Enabled by Localized High-Concentration Electrolytes. *Adv. Mater.* **2018,** *30* (21), e1706102.

(43) Ren, X.; Zou, L.; Cao, X.; Engelhard, M. H.; Liu, W.; Burton, S. D.; Lee, H.; Niu, C.; Matthews, B. E.; Zhu, Z.; Wang, C.; Arey, B. W.; Xiao, J.; Liu, J.; Zhang, J.-G.; Xu, W., Enabling High-Voltage Lithium-Metal Batteries under Practical Conditions. *Joule* **2019,** *3* (7), 1662-1676.

(44) Cao, X.; Gao, P.; Ren, X.; Zou, L.; Engelhard, M. H.; Matthews, B. E.; Hu, J.; Niu, C.; Liu, D.; Arey, B. W.; Wang, C.; Xiao, J.; Liu, J.; Xu, W.; Zhang, J. G., Effects of fluorinated solvents on electrolyte solvation structures and electrode/electrolyte interphases for lithium metal batteries. *Proc. Natl. Acad. Sci. U.S.A.* **2021,** *118* (9), e2020357118.

(45) Lin, L.; Qin, K.; Hu, Y. S.; Li, H.; Huang, X.; Suo, L.; Chen, L., A Better Choice to Achieve High Volumetric Energy Density: Anode-Free Lithium Metal Batteries. *Adv. Mater.* **2022,** e2110323.

(46) Li, K.; Zhang, J.; Lin, D.; Wang, D. W.; Li, B.; Lv, W.; Sun, S.; He, Y. B.; Kang, F.; Yang, Q. H.; Zhou, L.; Zhang, T. Y., Evolution of the electrochemical interface in sodium ion batteries with ether electrolytes. *Nat. Commun.* **2019,** *10* (1), 725.

(47) Zhou, X.; Zhang, Q.; Zhu, Z.; Cai, Y.; Li, H.; Li, F., Anion Reinforced Solvation for Gradient Inorganic-Rich Interphase Enables High-Rate and Stable Sodium Batteries. *Angew. Chem. Int. Ed.* **2022,** e202205045.

(48) Zhu, C.; Sun, C.; Li, R.; Weng, S.; Fan, L.; Wang, X.; Chen, L.; Noked, M.; Fan, X., Anion–Diluent Pairing for Stable High-Energy Li Metal Batteries. *ACS Energy Lett.* **2022,** 1338-1347.

(49) Zhang, X.; Zou, L.; Xu, Y.; Cao, X.; Engelhard, M. H.; Matthews, B. E.; Zhong, L.; Wu, H.; Jia, H.; Ren, X.; Gao, P.; Chen, Z.; Qin, Y.; Kompella, C.; Arey, B. W.; Li, J.; Wang, D.; Wang, C.; Zhang, J. G.; Xu, W., Advanced Electrolytes for Fast-Charging High-Voltage Lithium-Ion Batteries in Wide-Temperature Range. *Adv. Energy Mater.* **2020,** *10* (22), 2000368.

(50) Liu, S.; Ji, X.; Piao, N.; Chen, J.; Eidson, N.; Xu, J.; Wang, P.; Chen, L.; Zhang, J.; Deng, T.; Hou, S.; Jin, T.; Wan, H.; Li, J.; Tu, J.; Wang, C., An Inorganic-Rich Solid Electrolyte Interphase for Advanced Lithium-Metal Batteries in Carbonate Electrolytes. *Angew. Chem. Int. Ed.* **2021,** *60* (7), 3661-3671.

TOC Graphic